Nanoscale

PAPER

View Article Online
View Journal | View Issue

Cite this: *Nanoscale*, 2022, **14**, 14552

Single-molecule detection with enhanced Raman scattering of tungsten oxide nanostructure†

Yoshitaka Shingaya, *[a] Hirokazu Takaki, [b] Nobuhiko Kobayashi, [b] Masakazu Aono [a] and Tomonobu Nakayama *[a,b]

Received 1st July 2022,
Accepted 21st August 2022

DOI: 10.1039/d2nr03596k

rsc.li/nanoscale

We have found that tungsten oxide nanorods have a very large enhancement effect on Raman scattering. The nanorods with adsorbed ^{12}CO and ^{13}CO at the ratio of 1 : 1 were dispersed on a Si substrate and Raman mapping was performed. The Raman images of ^{12}CO and ^{13}CO were completely different, indicating that a very small number of molecules at the single-molecule level were observed. We also confirmed the characteristic blinking phenomenon when single-molecule detection was performed. The very large enhancement effect of Raman scattering can be attributed to the {001}CS structure of the tungsten oxide nanorods. It was confirmed from the DFT calculation results that the {001}CS structure exhibits two-dimensional electrical conduction properties.

1. Introduction

Raman scattering spectroscopy is a powerful method of identifying molecular species or obtaining information of the environment of molecules.[1] However, an extremely small cross section[2] of Raman scattering makes it difficult to realize single-molecule-level detection sensitivity, which is required for certain types of application such as medical diagnostics,[3] water or environmental monitoring[4] and food safety monitoring.[5] Surface enhanced Raman scattering (SERS) can greatly amplify Raman signals as already demonstrated using roughened surfaces of Ag, Au or Cu[6–8] or their nanoparticles. SERS with extremely high sensitivity has been realized with Ag nanoparticle aggregates, eventually demonstrating single-molecule-level detection sensitivity.[9–11] The extremely large enhancement effect observed is mainly due to the surface plasmon resonance in a nanogap region between two adjacent Ag nanoparticles.[12,13] Considerable efforts have been devoted so far to optimizing inter-nanoparticle distances[14–16] or shapes of noble-metal islands on insulating substrates[17] to maximize the enhancement effect. To date, metals for obtaining a substantial SERS effect have been limited to noble metals such as Ag and Au.

In recent years, plasmonics based on semiconducting materials such as metal oxides, metal chalcogenide and metal nitrides have attracted considerable attention.[18–20] Titanium nitride nanoparticles for photothermal conversion,[21] tunable localized surface plasmon resonance using indium tin oxide nanoparticles[22] or tungsten oxide nanocrystals,[23] epsilon-near-zero materials using tungsten bronze[24,25] and photo catalytic reaction using molybdenum oxide or tungsten oxide[26–28] have been reported. SERS effect using semiconducting nanocrystals has also been reported,[29–33] however, the enhancement factor is not very large and single-molecule detection is not achievable.

In this paper, we report that a metal oxide nanorod, an intermediate oxide of tungsten, WO_x ($x < 3$),[34–36] shows an extremely large enhancement effect of Raman scattering, and we also show that single-molecule detection becomes possible by using a certain activation procedure. Carbon monoxide (CO) adsorbed on WO_x is clearly detected through the C–O stretching peak in Raman spectra; however it is very difficult to observe Raman scattering from such an adsorbed molecule. We further show that WO_x enables us to detect even single-molecule through Raman spectroscopy. This result indicates that an extremely large enhancement effect of Raman scattering is indeed available with a metal oxide if it is appropriately engineered. WO_x ($x = 2.75$) is an atomically well-defined single crystal with two-dimensional conducting layers as revealed by our theoretical calculations.

[a]*International Center for Materials Nanoarchitectonics (WPI-MANA), National Institute for Materials Science (NIMS), 1-1 Namiki, Tsukuba 305-0044, Japan. E-mail: SHINGAYA.Yoshitaka@nims.go.jp, NAKAYAMA.Tomonobu@nims.go.jp*
[b]*Faculty of Pure and Applied Sciences, University of Tsukuba, 1-1-1 Tennodai, Tsukuba, Ibaraki 305-8573, Japan*

† Electronic supplementary information (ESI) available. See DOI: https://doi.org/10.1039/d2nr03596k

2. Results and discussion

The large enhancement effect of Raman scattering that enables the observation of adsorbed molecule originates from WO_x nanorod. Fig. 1a shows a scanning electron microscope

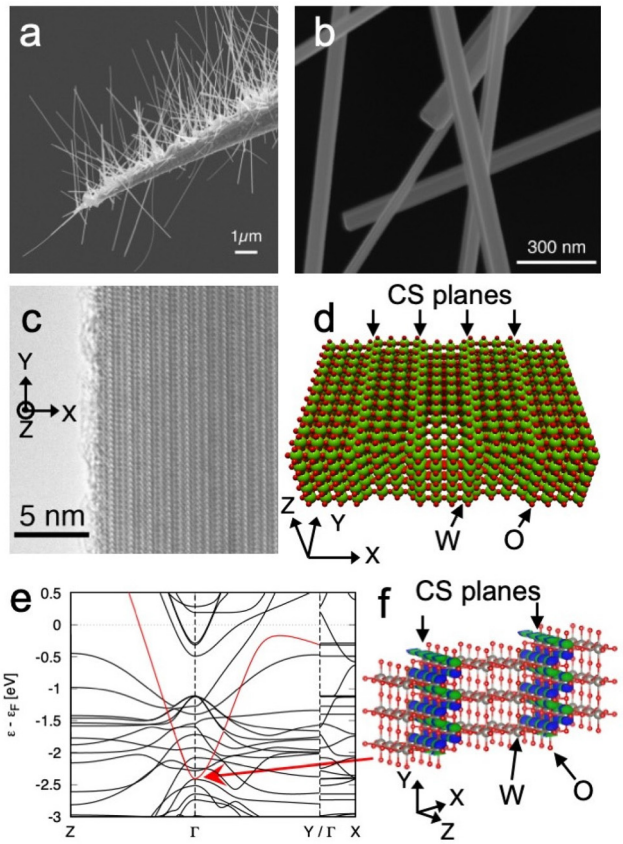

Fig. 1 (a) SEM image of WO_x nanorods on electrochemically sharpened tungsten tip. (b) Magnified SEM image of WO_x nanorods. (c) TEM image of WO_x nanorod. Observed image corresponds to W_4O_{11} that is intermediate oxide of tungsten with {001} type crystallographic shear (CS) structure. (d) Schematic representation of W_4O_{11} structure. Red spheres are oxygen atoms and Green spheres are tungsten atoms. (e) Band diagram for W_4O_{11}-CS structure obtained with density functional theory calculations. (f) Wave functions of the band indicated by the arrow.

(SEM) image of WO_x nanorods grown on an electrochemically etched tungsten tip. The length of the nanorods is typically 1–10 μm. The thickness of the WO_x nanorods is 20–150 nm, as can be determined from the SEM image shown in Fig. 1b. Fig. 1c shows a transmission electron microscope image of a WO_x nanorod. The nanorod has planar defects of oxygen inside. The periodic stacking of the planar defects forms the {001}-type crystallographic shear (CS) structure described as W_nO_{3n-1}. The observed structure corresponds to W_4O_{11}, which is one of the {001}CS structures.[34] A structural model of W_4O_{11}-CS is shown in Fig. 1d. Various intermediate oxides of tungsten show metallic conductivity.[37–39] However, the electrical conductivity of the {001}CS structure remains unclear. Therefore, we carried out the first-principles electronic structure calculation for the W_4O_{11}-CS structure on the basis of density functional theory. We obtained the electronic band structure by the localized atomic orbital basis set method implemented in SAKE.[40] We confirmed that the W_4O_{11}-CS structure exhibits a metallic band structure, as shown in Fig. 1e. A highly dispersive band that crosses the Fermi energy exists. The band has dispersion in the *yz* directions, but not in the *x* direction. This indicates two-dimensional conducting layers forming in the {001}CS structure. Our theoretical calculations showed that the wave function of that band localized in the CS plane as shown in Fig. 1f. It is expected that the plasmon resonance due to free electrons in the two-dimensional conducting layers may contribute to the enhancement of Raman scattering.

We found that Raman spectra obtained from WO_x nanorods contain Raman scattering attributable to adsorbed molecules, as will be shown later. Therefore, we expected that WO_x nanorods would have the enhancement effect of Raman scattering. Since the peak frequency of an adsorbed molecule largely changes from position to position, we expect that the number of observed molecules will be very small and WO_x nanorods will have an extremely large enhancement effect of Raman scattering. To prove this hypothesis, Raman spectroscopy was carried out for the WO_x nanorods exposed to a 1 : 1 mixture of two isotopes. We used adsorbed CO molecules to estimate the enhancement effect. The CO molecules on WO_x nanorods were formed by decomposition of 1 : 1 mixture of methanol-^{12}C and methanol-^{13}C in an ultra high vacuum (UHV) chamber.[41–43]

Fig. 2a shows accumulated Raman spectra of the adsorbed CO on WO_x nanorods formed by the decomposition of methanol. The spectra were obtained at 225 different points in a 9 μm × 8 μm area on densely grown WO_x nanorods, as indicated by the square in Fig. 2b. In this area, more than one hundred nanorods were included. Fig. 2b shows an optical microscope image of densely grown WO_x nanorods on the tungsten tip. The lower spectrum in Fig. 2a was obtained after exposing the nanorods to methanol-^{12}C at 600 °C and 5×10^{-5} torr for 15 min. Only the peak corresponding to ^{12}CO molecules was observed. The upper spectrum of Fig. 2a was obtained after exposing the nanorods to the 1 : 1 mixture of methanol-^{12}C and methanol-^{13}C at 640 °C and 5×10^{-5} torr for 10 min. Two peaks correspond to the adsorbed ^{13}CO and ^{12}CO. Since we observed CO molecules on a large number of WO_x nanorods in this case, the two peaks appear at a 1 : 1 ratio. The difference in vibrational frequency between the two peaks is reasonably attributed to the isotope substitution of the carbon atom of the CO molecules. Normally, it is very difficult to observe Raman scattering from such adsorbed molecules. We expected that the WO_x nanorods would have some enhancement effect of Raman scattering. Here, we note that as-grown nanorods did not show the Raman peak from CO molecules. After laser irradiation of 1 mW μm^{-2}, CO peaks appeared. Once the peaks corresponding to CO molecules appear in the Raman spectrum, it is possible to observe them even when the laser intensity is reduced. These results indicate that the activation by laser irradiation is required for detecting adsorbed molecules.

It is necessary to mention here the vibrational frequency of the adsorbed CO molecules observed in this study. The vibrational frequencies of observed CO molecules are much lower than that of adsorbed CO molecules shown in the pre-

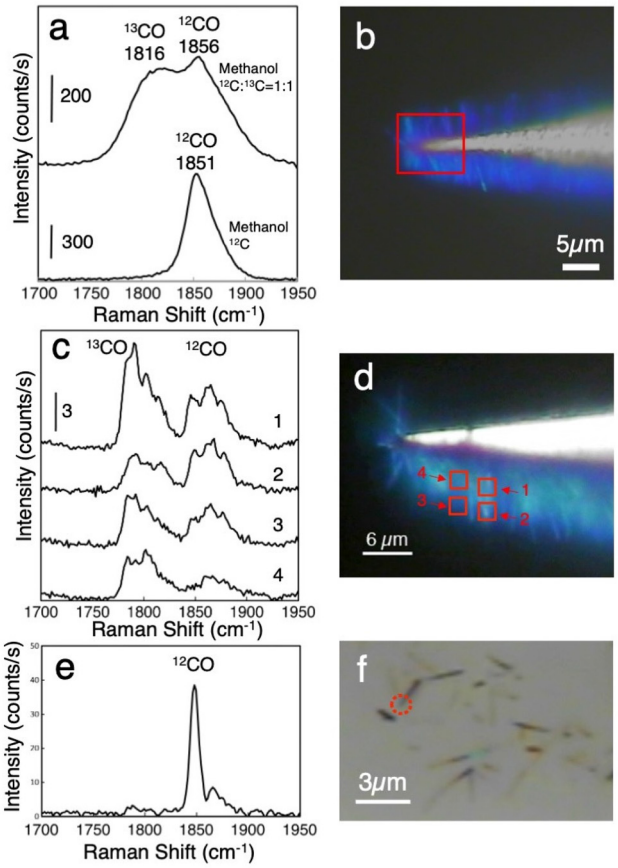

Fig. 2 (a) Raman scattering spectra of adsorbed CO on WO_x nanorods formed by decomposition of methanol. The spectra were obtained at 225 different points in a 9 μm × 8 μm area on densely grown WO_x nanorods as indicated by the square in (b). More than 100 nanorods are present in this region. The lower spectrum was obtained after exposing the nanorods to methanol-^{12}C at 600 °C and 5 × 10^{-5} torr for 15 min. The upper spectrum was obtained after exposing the nanorods to the 1 : 1 mixture of methanol-^{12}C and methanol-^{13}C at 640 °C and 5 × 10^{-5} torr for 10 min. Raman scattering measurements were carried out in air. (b) Optical microscope image of tungsten tip with densely grown WO_x nanorods. (c) Raman spectra of adsorbed CO from 20–50 of WO_x nanorods. (d) Optical microscope image of tungsten tip with densely grown WO_x nanorods. The four red squares indicate the observed areas of Raman spectra in (c). (e) Raman spectra of adsorbed CO from 1–3 of WO_x nanorods on Si substrate. (f) Optical microscope image of WO_x nanorods on Si substrate. Excitation laser: Ar^+ laser, 514.5 nm, 1.0 mW for (a and e) 0.1 mW for (c).

vious SERS measurements.[44] This is due to the difference in substrate materials. What is observed in the literature are CO molecules adsorbed on silver. CO molecules are weakly adsorbed on silver, therefore the intramolecular bonding of CO molecules is not very different from that of CO molecules in the gas phase. In contrast, CO molecules are strongly adsorbed on transition metals. As a result, the intramolecular bonding of CO become weaker and the intramolecular vibrations shift to lower frequencies. It is known that CO molecules adsorbed on the bridge site have a particularly large low frequency shift. The 1850 cm^{-1} obtained in the present study corresponds well to the peak position of CO molecules adsorbed on the bridge site of the transition metal surface.[45] As can be seen from the structural model in Fig. 1d, tungsten oxide nanorods with CS planes have bridge sites on the CS planes. It is considered that the CO molecules adsorbed on the bridge sites on the CS planes are observed in this study.

Fig. 2c shows Raman spectra from an intermediate number of WO_x nanorods. In this case, WO_x nanorods were exposed to 1 × 10^{-6} torr methanol for 100 seconds at room temperature after growth. To reduce the number of observed molecule, the number of accumulated pixels was reduced to 9 in a 2 μm × 2 μm area. In this area, 20–50 nanorods were included. Four spectra were obtained at different positions on densely grown WO_x nanorods, as shown in Fig. 2d with the correspondingly numbered squares. Although the 1 : 1 mixture of methanol-^{12}C and methanol-^{13}C was used in this case, the intensity ratio of ^{13}CO to ^{12}CO is not anymore 1 : 1. This indicates that the number of observed CO molecules was already very small. The appearance of multiple components in the CO stretching mode is due to a subtle difference between the adsorption states of CO on WO_x nanorods[46] that are averaged out when we observe many adsorbed molecules. Several components that originate from different adsorption sites appeared for a small number of adsorbed CO molecules. The intensity ratio differed from position to position.

To further reduce their number, WO_x nanorods were dispersed on a Si substrate, and Raman spectra were observed from 1–3 WO_x nanorods. Fig. 2e shows the Raman spectra obtained at the single point indicated by the red circle in Fig. 2f. In this case, the intensity ratio of ^{12}CO to ^{13}CO increases further. Almost no ^{13}CO peak appears except for a small peak at 1783 cm^{-1}, whereas a very sharp and intense peak at 1848 cm^{-1} and a smaller peak at 1862 cm^{-1} appear for ^{12}CO. Since the ratio of ^{12}CO to ^{13}CO should be 1 : 1 if the Raman spectra correspond to many molecules, this result strongly suggests that single-molecule-level observation becomes possible for adsorbed CO.

To prove the single-molecule Raman scattering observation with an extremely large enhancement effect of WO_x nanorods more clearly, Raman mapping was conducted for WO_x nanorods with a 1 : 1 isotope mixture of CO. Fig. 3a and b show optical microscope and SEM images of WO_x nanorods dispersed on a Si substrate. Fig. 3c and e respectively show Raman mappings of the ^{13}CO and ^{12}CO peaks obtained at the same area as in Fig. 3a and b. The result of mapping for the ^{13}CO peak is totally different from that for the ^{12}CO peak. Fig. 3d and f show the spectra obtained at the positions indicated by circles in Fig. 3c and e. We observed that only one isotope appears in each spectrum. This indicates that the observed peaks originate from a very small number of CO molecules, that is, the single-molecule-level.

As mentioned above, as-grown nanorods did not show a large enhancement effect of Raman scattering to enable single-molecule detection. After laser irradiation as intense as 0.1–1.5 mW $μm^{-2}$, single-molecule detection became possible. The threshold intensities of activation were dependent on the

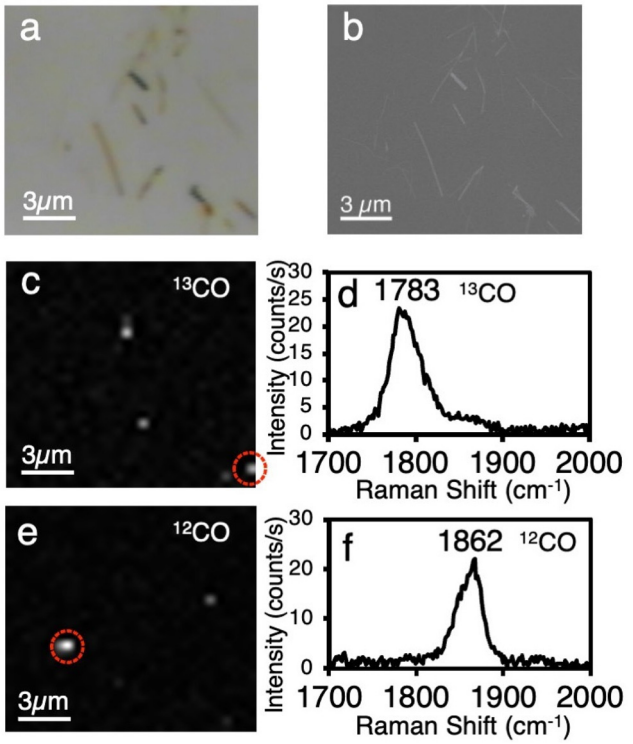

Fig. 3 (a) Optical microscope image and (b) scanning electron microscope image of WO_x nanorods on Si substrate. Raman mappings of (c) ^{13}CO and (e) ^{12}CO measured in the same area as in (a and b). (d and f) Show Raman spectra obtained at the positions indicated by circles in (c and e). Excitation laser: Ar^+ laser, 514.5 nm, 1.0 mW.

diameter and position of WO_x nanorods. Nanorods with larger diameters tend to be activated at a lower intensity of an irradiated laser. In addition, the laser irradiation near the end of a nanorod can activate the nanorod of a lower laser power than the irradiation in the center of the nanorod. This activation procedure corresponds to cutting the CS planes by the local oxidation of WO_x and localizing the plasmon at the active site formed by the oxidation.

It should be mentioned here that the enhancement factor (EF) become very large, over 10^{10}. The calculation of the EF is described in ESI.† CO molecules do not have absorption in the visible light region. Therefore, the resonance Raman effect is not expected. We consider that this very large enhancement factor is mainly caused by the electromagnetic mechanism due to plasmon resonance. The results of additional experiments supporting this explanation are shown in Fig. S1 and S2 in ESI.† The light scattering spectrum obtained from a single WO_x nanorod is shown in Fig. S1.† The light scattering with a peak around 450 nm is attributed to the plasmon resonance of the WO_x nanorod. When the light within the peak wavelength region of the light scattering spectrum is used as the excitation light for Raman scattering, a large enhancement effect is obtained. Fig. S2† shows the results of electrical measurements of a single tungsten oxide nanorod using the prober in the SEM. A completely linear *IV* curves were obtained, indicating that the WO_x nanorods have metallic electrical properties. The electrical resistivity determined from the diameter and the length of the nanorod was quite low, 2.9×10^{-4} Ω cm. These results support electromagnetic mechanism due to plasmon resonance. There is possibility that charge transfer mechanism also contribute to the large enhancement effect. The details of the enhancement mechanism are not yet clear, and are considered to be a target for future work.

The enhanced Raman scattering of adsorbed CO on WO_x nanorods shows time-dependent spectral changes, that is, the so-called blinking phenomenon. As the blinking is characteristic of single-molecule observation,[9,47–49] the following result is additional evidence that the observed CO is at the single-molecule level. Fig. 4a shows time series Raman spectra of adsorbed CO on WO_x nanorods dispersed on the Si substrate acquired at 1.5 s intervals. In this case also, ^{13}CO and ^{12}CO exist at a 1 : 1 ratio on WO_x nanorods. Fig. 4b indicates the Raman spectra obtained at various times. A peak at 1772 cm^{-1} corresponds to ^{13}CO molecule and peaks at 1855 and 1886 cm^{-1} correspond to ^{12}CO molecules. The large difference in peak intensity between ^{13}CO and ^{12}CO indicates that the number of observed CO molecules is very small (single-molecule level). The peak at 1772 cm^{-1} comes from single ^{13}CO molecule, and it shows time-dependent changes in its intensity and position. These time-dependent changes are due to change of adsorption site of CO. At t = 48.5 s an intense peak appears at 1745 cm^{-1}. The peak rapidly disappears because of the instability of the adsorption state that causes a rather low vibrational frequency of CO. After this event, a shoulder peak appears at 1795 cm^{-1}. Fig. 4c shows plots of peak intensities

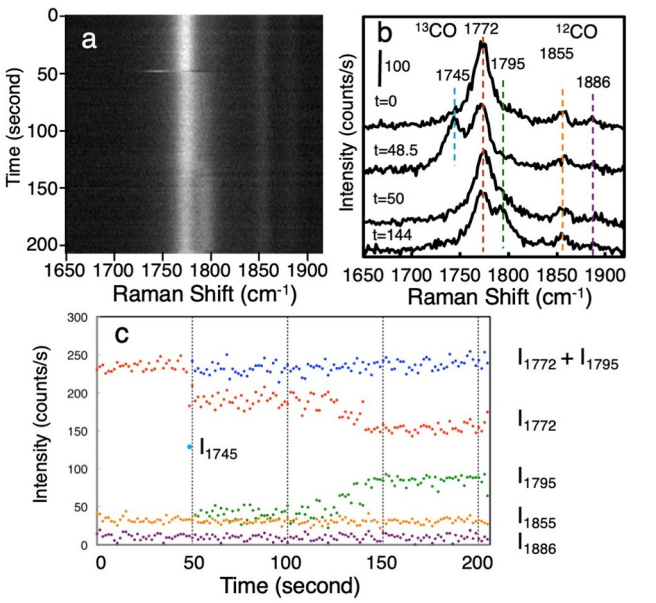

Fig. 4 (a) Time series Raman spectra of adsorbed CO on WO_x nanorods dispersed on Si substrate acquired at 1.5 s intervals. (b) Raman spectra obtained at t = 0, 48.5, 50 and 144 s. (c) Peak intensity plots as a function of time. Excitation laser: Ar^+ laser, 514.5 nm, 1.0 mW.

as a function of time. The peak intensities of each peak were obtained by peak fitting. Although the peak intensities of ^{12}CO at 1855 and 1886 cm^{-1} were constant throughout the measurements, the peak intensity of ^{13}CO at 1772 cm^{-1} drastically changed. The splitting of the peak starting at t = 48.5 s corresponds to the rapid hopping of CO molecule between two adsorption states. The peak intensity indicates the occupation time of each adsorption state. The peak intensity at 1772 cm^{-1} gradually decreases from t = 124 s, whereas the peak intensity at 1795 cm^{-1} increases. The total intensity of peaks at 1772 cm^{-1} and 1795 cm^{-1} was almost constant after the start of splitting at t = 48.5 s. This result clearly indicates the negative correlation between two peaks and can be explained by the variation of the occupation time between two different adsorption states. When we observe thousands of molecules using a conventional spectroscopic technique, such detailed information of adsorption states is averaged out. Single-molecule detection with a large enhancement effect of Raman scattering enables us to examine in detail the dynamic behavior of the bonding state and environmental conditions of the target molecule.

3. Conclusions

We have found that WO_x nanorods show an extremely large enhancement effect of Raman scattering, and the vibrational spectra of a single adsorbed CO molecule become observable. Although as-grown nanorods did not show a large enhancement effect of Raman scattering, after laser irradiation at an intensity of 0.1–1.5 mW μm^{-2}, single-molecule detection became possible. This activation procedure corresponds to cutting the CS planes by the local oxidation of WO_x, and the locally oxidized part works as the active site for Raman enhancement. The Raman mapping of the isotope mixture proved the detection of a single molecule. The Raman mapping was performed for nanorods with adsorbed ^{12}CO and ^{13}CO at the ratio of 1 : 1. The Raman images of ^{12}CO and ^{13}CO were completely different, indicating that a very small number of molecules at the single-molecule level were observed. DFT calculations revealed the existence of a 2D conducting layer at the CS plane. Therefore, we considered that plasmon resonance using free electrons in 2D conducting layers in WO_x nanorods is the main factor for the large enhancement effect. Conventional single-molecule SERS is always realized in a nearly closed system such as a nanogap or nanocavity. In contrast, the enhancement of Raman scattering by WO_x is expected to be realized at the cleavage site of conducting planes at the surfaces of nanorods. It is considered that the active sites of Raman enhancement can be brought into close proximity to macromolecules such as proteins. Therefore, this technique has the potential to greatly expand the application of single-molecule SERS. WO_x nanorods can be attached to the apex of probe for a scanning probe microscope.[50] Therefore, chemical analysis with extremely high spatial resolution is expected to realize.

4. Experimental section

We have already developed an epitaxial growth technique for WO_x nanorods on tungsten in a UHV chamber.[50–52] The WO_x nanorods were grown on electrochemically etched tungsten substrates. The substrates were annealed at 1100 °C to remove the residual oxide layer on the surface. Then the substrate was kept at 700 °C to 850 °C. Oxygen gas at 5×10^{-6} torr was introduced into the chamber, and the tungsten foil heated at 1100 °C was placed in front of the substrate in order to deposit tungsten oxide on the substrate. The growth time was 5 to 10 h. The obtained tungsten oxide showed a nanorod shape.

Raman scattering spectral measurements were performed in air with a micro-Raman system (HORIBA Jobin-Yvon, HR-800) using an Ar-ion laser of 514.5 nm wavelength for excitation focused in a 1 μm diameter spot with a 100× objective lens (Olympus, 0.90 numerical aperture). The light that scattered back from the sample was collected with the same objective lens and detected through a polychromator with a liquid-nitrogen-cooled CCD camera. Detailed structures of WO_x nanorods were observed by field emission-SEM (JEOL JSM-6500F) and TEM (JEOL JEM-2000EX). Highly pure oxygen gas (99.99995%) was used for WO_x nanorod growth. Deuterated methanol-^{12}C,^{13}C (Cambridge Isotope Laboratories) was used for the formation of adsorbed molecules.

Author contributions

The manuscript was written by Y. S. and T. N. through the support of all the co-authors. Y. S. performed growth and characterization of WO_x nanorods. Y. S. performed micro-Raman measurements. H. T. and N. K. performed theoretical calculations. N. K. and M. A. discussed band structure and possible enhancement mechanism. All the authors analyzed the data, discussed the results and commented on the manuscript.

Conflicts of interest

The authors declare no conflicts of interest.

Acknowledgements

We would like to thank Dr K. Kurashima for TEM observation. This study was supported by the World Premier International Center (WPI) for Materials Nanoarchitectonics (MANA) of the National Institute for Materials Science (NIMS), Tsukuba, Japan, and JSPS Kakenhi grant number 20K05280.

References

1 S. Schlucker, *Angew. Chem., Int. Ed.*, 2014, **53**, 4756–4795.
2 E. C. Le Ru and P. G. Etchegoin, *Annu. Rev. Phys. Chem.*, 2012, **63**, 65–87.

3 M. Mascini and S. Tombelli, *Biomarkers*, 2008, **13**, 637–657.
4 C. I. L. Justino, A. C. Duarte and T. A. P. Rocha-Santos, *Sensors*, 2017, **17**, 2918–2943.
5 Z. Lin and L. He, *Curr. Opin. Food Sci.*, 2019, **28**, 82–87.
6 M. Fleischmann, P. J. Hendra and A. J. McQuillan, *Chem. Phys. Lett.*, 1974, **26**, 163–166.
7 D. L. Jeanmaire and R. P. Van Duyne, *J. Electroanal. Chem.*, 1977, **84**, 1–20.
8 M. G. Albrecht and J. A. Creighton, *J. Am. Chem. Soc.*, 1977, **99**, 5215–5217.
9 S. Nie and S. R. Emory, *Science*, 1997, **275**, 1102–1106.
10 K. Kneipp, Y. Wang, H. Kneipp, L. T. Perelman, I. Itzkan, R. R. Dasari and M. S. Feld, *Phys. Rev. Lett.*, 1997, **78**, 1667–1670.
11 H. Xu, E. J. Bjerneld, M. Käll and L. Börjesson, *Phys. Rev. Lett.*, 1999, **83**, 4358–4360.
12 M. Moskovits, *Rev. Mod. Phys.*, 1985, **57**, 783–826.
13 T. Itoh, Y. S. Yamamoto and Y. Ozaki, *Chem. Soc. Rev.*, 2017, **46**, 3904–3921.
14 G. J. Kovacs, R. O. Loutfy, P. S. Vincett, C. Jennings and R. Aroca, *Langmuir*, 1986, **2**, 689–694.
15 E. W. A. Visser, M. Horacek and P. Zijlstra, *Nano Lett.*, 2018, **18**, 7927–7934.
16 J. F. Li, Y. F. Huang, Y. Ding, Z. L. Yang, S. B. Li, X. S. Zhou, F. R. Fan, W. Zhang, Z. Y. Zhou, D. Y. Wu, B. Ren, Z. L. Wang and Z. Q. Tian, *Nature*, 2010, **464**, 392–395.
17 C. L. Haynes and R. P. Van Duyne, *J. Phys. Chem. B*, 2001, **105**, 5599–5611.
18 A. Comin and L. Manna, *Chem. Soc. Rev.*, 2014, **43**, 3957–3975.
19 G. V. Naik, V. M. Shalaev and A. Boltasseva, *Adv. Mater.*, 2013, **25**, 3264–3294.
20 I. Kriegel, F. Scotognella and L. Manna, *Phys. Rep.*, 2017, **674**, 1–52.
21 S. Ishii, R. P. Sugavaneshwar and T. Nagao, *J. Phys. Chem. C*, 2016, **120**, 2343–2348.
22 M. Kanehara, H. Koike, T. Yoshinaga and T. Teranishi, *J. Am. Chem. Soc.*, 2009, **131**, 17736–17737.
23 K. Manthiram and A. P. Alivisatos, *J. Am. Chem. Soc.*, 2012, **134**, 3995–3998.
24 L. Tegg, D. Cuskelly and V. J. Keast, *Plasmonics*, 2017, **13**, 437–444.
25 Z. Fusco, M. Taheri, R. Bo, T. Tran-Phu, H. Chen, X. Guo, Y. Zhu, T. Tsuzuki, T. P. White and A. Tricoli, *Nano Lett.*, 2020, **20**, 3970–3977.
26 H. Cheng, M. Wen, X. Ma, Y. Kuwahara, K. Mori, Y. Dai, B. Huang and H. Yamashita, *J. Am. Chem. Soc.*, 2016, **138**, 9316–9324.
27 X. Zhang, X. Wang, X. Yi, L. Liu, J. Ye and D. Wang, *ACS Appl. Energy Mater.*, 2020, **3**, 3569–3576.
28 G. Xi, S. Ouyang, P. Li, J. Ye, Q. Ma, N. Su, H. Bai and C. Wang, *Angew. Chem., Int. Ed.*, 2012, **51**, 2395–2399.
29 W. Li, R. Zamani, P. Rivera Gil, B. Pelaz, M. Ibanez, D. Cadavid, A. Shavel, R. A. Alvarez-Puebla, W. J. Parak, J. Arbiol and A. Cabot, *J. Am. Chem. Soc.*, 2013, **135**, 7098–7101.
30 L. Jiang, T. You, P. Yin, Y. Shang, D. Zhang, L. Guo and S. Yang, *Nanoscale*, 2013, **5**, 2784–2789.
31 A. Musumeci, D. Gosztola, T. Schiller, N. M. Dimitrijevic, V. Mujica, D. Martin and T. Rajh, *J. Am. Chem. Soc.*, 2009, **131**, 6040–6041.
32 D. Qi, L. Lu, L. Wang and J. Zhang, *J. Am. Chem. Soc.*, 2014, **136**, 9886–9889.
33 S. Cong, Y. Yuan, Z. Chen, J. Hou, M. Yang, Y. Su, Y. Zhang, L. Li, Q. Li, F. Geng and Z. Zhao, *Nat. Commun.*, 2015, **6**, 7800.
34 G. L. Frey, A. Rothschild, J. Sloan, R. Rosentsveig, R. Popovitz-Biro and R. Tenne, *J. Solid State Chem.*, 2001, **162**, 300–314.
35 Y. Q. Zhu, H. Weibing, W. K. Hsu, M. Terrones, N. Grobert, P. H. Jonathan, H. W. Kroto, D. R. M. Walton and H. Terrones, *Chem. Phys. Lett.*, 1999, **309**, 327–334.
36 J. Sloan, J. L. Hutchison, R. Tenne, Y. Feldman, T. Tsirlina and M. Homyonfer, *J. Solid State Chem.*, 1999, **144**, 18.
37 W. Sahle and M. Nygren, *J. Solid State Chem.*, 1983, **48**, 154–160.
38 M. Remškar, J. Kovac, M. Viršek, M. Mrak, A. Jesih and A. Seabaugh, *Adv. Funct. Mater.*, 2007, **17**, 1974–1978.
39 K. Viswanathan, K. Brandt and E. Salje, *J. Solid State Chem.*, 1981, **36**, 45–51.
40 H. Takaki, N. Kobayashi and K. Hirose, *J. Phys.: Condens. Matter*, 2020, **32**, 325901.
41 J. Hrbek, R. A. DePaola and F. M. Hoffmann, *J. Chem. Phys.*, 1984, **81**, 2818–2827.
42 K. Franaszczuk, E. Herrero, P. Zelenay, A. Wieckowski, J. Wang and R. I. Masel, *J. Phys. Chem.*, 1992, **96**, 8509–8516.
43 R. Brito de Barros, A. R. Garcia and L. M. Ilharco, *Surf. Sci.*, 2003, **532–535**, 185–190.
44 I. Mrozek, C. Pettenkofer and A. Otto, *Surf. Sci.*, 1990, **238**, 192–198.
45 H. Hopster and H. Ibach, *Surf. Sci.*, 1978, **77**, 109–117.
46 A. Kudelski and B. Pettinger, *Chem. Phys. Lett.*, 2004, **383**, 76–79.
47 S. M. Stranahan and K. A. Willets, *Nano Lett.*, 2010, **10**, 3777–3784.
48 J. A. Dieringer, R. B. Lettan II, K. A. Scheidt and R. P. Van Duyne, *J. Am. Chem. Soc.*, 2007, **129**, 16249–16256.
49 Y. Sharaabi, T. Shegai and G. Haran, *Chem. Phys.*, 2005, **318**, 44–49.
50 O. Kubo, Y. Shingaya, M. Nakaya, M. Aono and T. Nakayama, *Appl. Phys. Lett.*, 2006, **88**, 254101–254103.
51 Y. Shingaya, T. Nakayama and M. Aono, *Sci. Technol. Adv. Mater.*, 2004, **5**, 647–649.
52 T. Nakayama, O. Kubo, Y. Shingaya, S. Higuchi, T. Hasegawa, C.-S. Jiang, T. Okuda, Y. Kuwahara, K. Takami and M. Aono, *Adv. Mater.*, 2012, **24**, 1675–1692.